

Generation of Plasmonic Vortex with Linearly Polarized Light

Feng Huang^{1,2} · Xiangqian Jiang^{1,2} · Haiming Yuan^{1,2} · Xiudong Sun^{1,2}

Received: 15 April 2016 / Accepted: 29 June 2016 / Published online: 12 July 2016
© Springer Science+Business Media New York 2016

Abstract A nanoslit-arrayed plasmonic lens that can generate plasmonic vortex with linearly polarized light is theoretically and numerically studied. The topological charge (TC) of generated plasmonic vortex is the sum of the geometrical charge of the proposed plasmonic lens and additional angular momentum of ± 1 . The plasmonic vortex is determined by the pitch of the plasmonic lens, the nanoslit rotation directions, as well as the polarization direction of the incident light. Combination of the geometry parameters of the plasmonic lens and the polarization direction of linearly polarized incident light, plasmonic vortices with arbitrary TC are flexibly generated. Moreover, by cutting the continuous nanoslit arrays into segments, highly ordered plasmonic vortices are realized with small plasmonic lens size. Comparisons with two slit plasmonic lenses are also presented to demonstrate the unique properties of the proposed plasmonic lens in plasmonic vortex generation.

Keywords Surface plasmon polaritons · Plasmonic lens · Plasmonic vortex

Introduction

Surface plasmon polaritons (SPP) are surface electromagnetic waves coupled with collective oscillation of electrons at

metal-dielectric interfaces [1]. The unique properties of SPP such as field localization and enhancement make them have a broad range of applications from sensing, lithography, and photovoltaic devices to integrated optical devices [2–5]. In recent years, the SPP-based plasmonic vortex has attracted much research interest [6–14], which is a near-field pattern having a Bessel function distribution with a spiral phase distribution at the interface of metal and dielectric. The plasmonic vortex has various applications such as optical tweezers, light focusing, and ultra-thin optical vortex plates [14–17]. Various plasmonic geometries have been presented to generate plasmonic vortex, such as plasmonic rings [18, 19], plasmonic Archimedes spiral [20, 21], chiral plasmonic slits [7, 10, 22], and nanoslit-arrayed plasmonic lenses [16, 23, 24]. However, the excitation of SPP is highly sensitive to the polarization state of incident light. Usually, only the component of incident light that is polarized perpendicularly to the metallic ridges or slits can be coupled into SPP [25]. To excite plasmonic vortex, radially polarized beam and vortex beam with spin and orbital angular momentums are utilized [7, 10, 18, 22]. Nevertheless, it is of less practicality because the preparation of radially polarized beam or vortex beam typically requires a complicated setup and the center of the beam and the plasmonic lens must coincide. Moreover, circularly polarized light with spin angular moment of ± 1 are utilized to generate plasmonic vortex [7, 9, 10, 20]. However, due to the SPP polarization sensitivity, it is difficult to generate plasmonic vortex with linearly polarized light.

In this paper, we propose a nanoslit-arrayed plasmonic lens that can generate arbitrarily ordered plasmonic vortex with linearly polarized incident light. The principle and the plasmonic vortex generation properties are theoretically and numerically analyzed. The overall effects of the geometric parameters and the polarization state of incident light on plasmonic vortex generation are studied. By cutting the

✉ Xiudong Sun
xdsun@hit.edu.cn

¹ Department of Physics, Harbin Institute of Technology, Harbin 150001, China

² Key Lab of Micro-Optics and Photonic Technology of Heilongjiang Province, Harbin 150001, China

continuous nanoslit arrays into segments, highly ordered plasmonic vortices are realized with a small plasmonic lens size. Moreover, for comparison, two conventional plasmonic lenses with linearly polarized incident light are numerically simulated.

Structure and Theoretical Analysis

The proposed plasmonic lens is schematically shown in Fig. 1. Two arrays of nanoslits are etched in a thin gold film on a SiO₂ substrate. The plasmonic lens is illuminated by a plane wave from the bottom of the SiO₂ substrate with normal incidence. The SPP launched at the air/gold interface is supposed to generate plasmon vortex at the center of the plasmonic lens with linearly polarized incident light. The top view of the plasmonic lens is shown in Fig. 1b. The two arrays of nanoslits are bent to Archimedes curves. The inner curve is described as follows:

$$r = r_0 + n\lambda_{\text{SPP}} \frac{\phi}{2\pi} \quad (1)$$

where r_0 is the minimum radius of the curve and λ_{SPP} is the SPP wavelength. The maximum radius of the curve is $r_0 + n\lambda_{\text{SPP}}$. Positive and negative n values denote a right-handed and a left-handed spiral, respectively. The distance between the two nanoslit arrays is D . The nanoslits in the inner and outer arrays are oriented at angles α_0 and $\alpha_0 + 90^\circ$ with respect to the x axis, respectively. The distances between adjacent nanoslits along the Archimedes curves in the same array are nearly the same and labeled as S . The two arrays of nanoslits are offset by $S/2$ along the Archimedes curves to reduce near-field coupling and scattering of the SPP by neighboring nanoslits [25].

Here, we define a local u - v coordinate system as shown in Fig. 1b. The origin is at the center of a nanoslit on top of the gold film. The u and v axes are parallel and perpendicular to the longer edge of the inner nanoslit, respectively. For a linearly polarized light with polarization angle ψ with respect to

the x axis, the polarization state can be expressed as the combination of two orthogonally and linearly polarized polarizations as follows:

$$\begin{aligned} \vec{E}_\psi = E_0 \cos\psi \hat{x} + E_0 \sin\psi \hat{y} = E_0 \cos(\psi - \alpha_0) \hat{u} \\ + E_0 \sin(\psi - \alpha_0) \hat{v} \end{aligned} \quad (2)$$

When the size of the nanoslits is considerably smaller than the wavelength of incident light, the nanoslits serve as SPP point sources. Moreover, when the nanoslits are narrow enough, only the component of the incident light that is polarized perpendicularly to the longer edge of the nanoslits can be coupled into SPP. Assuming the structure is large enough and the nanoslits are arrayed closely, the coupled SPP near the inner nanoslit array is proximately given by the following [26]:

$$\begin{aligned} \vec{E}_{\text{SPP}}^\psi = E_0 \sin(\psi - \alpha_0) C e^{-k_z z} \cos(\phi + \alpha_0) \hat{z} \\ + E_0 \cos(\psi - \alpha_0) C e^{-k_z z} \cos(\phi + \alpha_0 + \pi/2) \cdot \exp(ik_{\text{SPP}} D) \hat{z} \end{aligned} \quad (3)$$

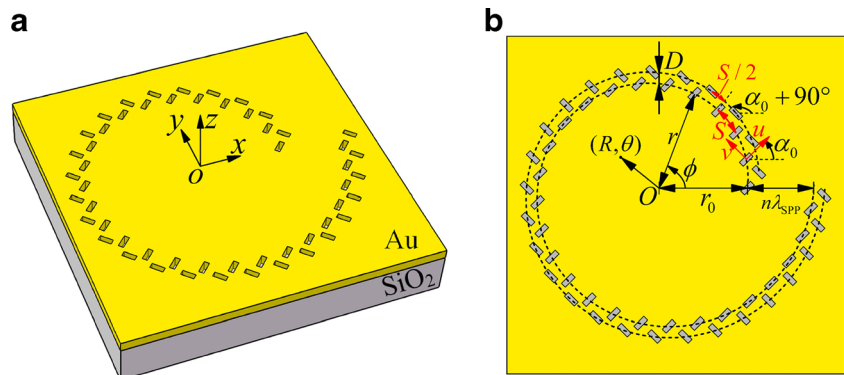
where C is the coupling coefficient, k_{SPP} is the wave vector of SPP, and $k_z = (k_{\text{SPP}}^2 - k_0^2)^{1/2}$ is the wave vector along z axis. Neglecting the propagation loss of SPP and setting $D = \lambda_{\text{SPP}}/4$, we get the following:

$$\vec{E}_{\text{SPP}}^\psi = \mp \frac{1}{\sqrt{2}} E_0 C e^{-k_z z} e^{\pm i(\phi + \alpha_0)} \hat{z} \quad (4)$$

where the minus and plus signs correspond to $\psi = \alpha_0 - 45^\circ$ and $\psi = \alpha_0 + 45^\circ$, respectively. For linearly polarized light, the angular momentum is zero. However, with the proposed plasmonic lens, the coupled SPP near the inner nanoslit array has a phase term of $e^{\pm i\phi}$ along the azimuthal direction in Eq. (4), which means that an additional angular momentum of ± 1 is generated.

The SPP excitations near the inner nanoslit array could act as secondary sources. By integrating the secondary sources

Fig. 1 **a** A 3D illustration of the proposed plasmonic lens, which consists of two arrays of nanoslits etched in a thin gold film on a SiO₂ substrate. **b** Top view of the proposed plasmonic lens



along the inner curve, the electric field at a point (R, θ) near the center of the structure can be calculated as follows [20, 22]:

$$\begin{aligned} \vec{E}_{\text{SPP}}(R, \theta) &= \int_0^{2\pi} \vec{E}_{\text{SPP}}^{\psi} e^{i\vec{k}_r \cdot (R\vec{e}_R - r\vec{e}_r)} r d\phi \quad (5) \\ &= \int_0^{2\pi} \frac{1}{\sqrt{2}} E_0 C e^{-k_z z} e^{\pm i\alpha_0} e^{\pm i\phi} e^{i\vec{k}_r \cdot (R\vec{e}_R - r\vec{e}_r)} r d\phi \end{aligned}$$

Neglecting the propagation loss of SPP and using $\vec{k}_r = -k_{\text{SPP}} \vec{e}_r$, we have the following:

$$\begin{aligned} \vec{E}_{\text{SPP}}(R, \theta) &= \mp \hat{z} \frac{1}{\sqrt{2}} E_0 C e^{-k_z z} e^{\pm i\alpha_0} \int_0^{2\pi} e^{\pm i\phi} e^{iRk_{\text{SPP}} \cos(\theta-\phi)} e^{ik_{\text{SPP}}r} r d\phi \\ &= \mp \hat{z} \sqrt{2\pi} E_0 C e^{-k_z z} r_0 e^{i(k_{\text{SPP}}r_0 \pm \alpha_0)} e^{i(n \pm 1)\theta} J_{n \pm 1}(k_{\text{SPP}}R) \quad (6) \end{aligned}$$

and the intensity distribution inside the plasmonic lens is as follows:

$$I(R, \theta) = 2\pi^2 I_0 C^2 e^{-2k_z z} r_0^2 |J_{n \pm 1}(k_{\text{SPP}}R)|^2 \quad (7)$$

where the Archimedes curve equation given in Eq. (1) is used and the structure is assumed to be large enough with respect to λ_{SPP} so that its size can be approximated with r_0 . $J_{n \pm 1}$ is the $(n \pm 1)$ th Bessel function of the first kind, and the order $n \pm 1$ denotes the topological charge (TC) of the generated plasmonic vortex field. The TC of the generated plasmonic vortex is the geometrical charge of the plasmonic lens n add or minus 1, corresponding to the polarization angle $\psi = \alpha_0 - 45^\circ$ or $\psi = \alpha_0 + 45^\circ$, respectively.

Simulation Results and Discussion

To check the theoretical analysis, simulations using finite element software COMSOL Multiphysics are performed. In the simulations, the refractive index of gold is taken from reference [27] and that of SiO_2 is 1.45. The incident wavelength λ is 800 nm. The SPP wavelength λ_{SPP} is 782 nm. The thickness of the gold film is 200 nm. The distance between the adjacent nanoslits is $S = 400$ nm. The distance between the two Archimedes curves is $D = \lambda_{\text{SPP}}/4 = 195.5$ nm. The size of all nanoslits is $250 \text{ nm} \times 60 \text{ nm}$. The calculation region is a cylinder with diameter of 12λ and height of 4λ . The bottom surface is incident boundary and set with scattering boundary condition. The top surface is set with perfectly matched layer adsorbing boundary condition, and the remaining surfaces are set with scattering boundary condition. Non-uniform mesh with maximum cell size of 10 nm for the nanoslit region and that of $\lambda/12$ at the air/gold interface is applied to guarantee the simulation accuracy.

The simulated results are shown in Fig. 2. The nanoslits in the inner and outer arrays are oriented at angles 45° and 135° with respect to the x axis, respectively ($\alpha_0 = 45^\circ$). According to the theoretical analysis, plasmonic vortex field with TC of $n \pm 1$ can be generated for 0° and 90° linearly polarized incident light, respectively. The first and second rows of Fig. 2 show the intensity $|E_z|^2$ distributions at the gold film top surface ($z=0$ plane) for $\psi=0^\circ$ and 90° linearly polarized incident light, respectively. The third and fourth rows of Fig. 2 are the E_z phase distributions at $z=0$ plane which correspond to the first and second rows of Fig. 2, respectively. From the left to the right columns, the pitch of the plasmonic lens varies from $-\lambda_{\text{SPP}}$ to $2\lambda_{\text{SPP}}$ with an increment of λ_{SPP} (n varies from -1 to 2). As expected, plasmonic vortexes are successfully generated. The TC of the generated plasmonic vortex is confirmed by comparing the primary ring size and the phase variation along the azimuthal direction in the center of the plasmonic lens [9, 22]. The TCs of generated plasmonic vortexes for $\psi=0^\circ$ linear polarization incidence are 0 to $+3$, while those for $\psi=90^\circ$ linear polarization incidence are -2 to $+1$. The simulation results agree well with the theoretical analysis. When the TC of the plasmonic vortex is 0, the field near the center of the plasmonic lens is centrally symmetric with a bright spot at the origin, as shown in Fig. 2a, g. The phase distributions are patterned with concentric circles, as shown in Fig. 2i, o. The full width at half maximum of the focal spot is about 280 nm ($\sim 0.35\lambda$). When the TC of the plasmonic vortex is not zero, the intensity distributions are also centrally symmetric but with dark centers, as shown in Fig. 2b–f, h. The size of the dark center increases with the TC of the plasmonic vortex. The phase distributions near the center of the plasmonic lens vary the TC times of 2π along the azimuthal direction, as shown in Fig. 2j–n, p. The rotation directions of the phase distributions near the center of the plasmonic lens are clockwise and anticlockwise which correspond to the positive and negative TC.

Moreover, the plasmonic vortex also depends on the orientation direction of the nanoslits. Figure 3a shows the intensity $|E_z|^2$ distribution at $z=0$ plane with $n=1$ and $\psi=0^\circ$ linear polarization incidence, but the orientation of all nanoslits is altered by 90° with respect to those in Fig. 2c. In other words, the nanoslits in the inner and outer arrays are oriented at angles 135° and 45° with respect to the x axis, respectively ($\alpha_0 = 135^\circ$). Compared with the intensity and phase distributions shown in Fig. 2c, k, it is found that the TC of generated plasmonic vortex changes from $+2$ to 0. Such phenomenon can be easily explained by changing α_0 from 45° to 135° , and the minus and plus signs in Eq. (4) is reversed for the same

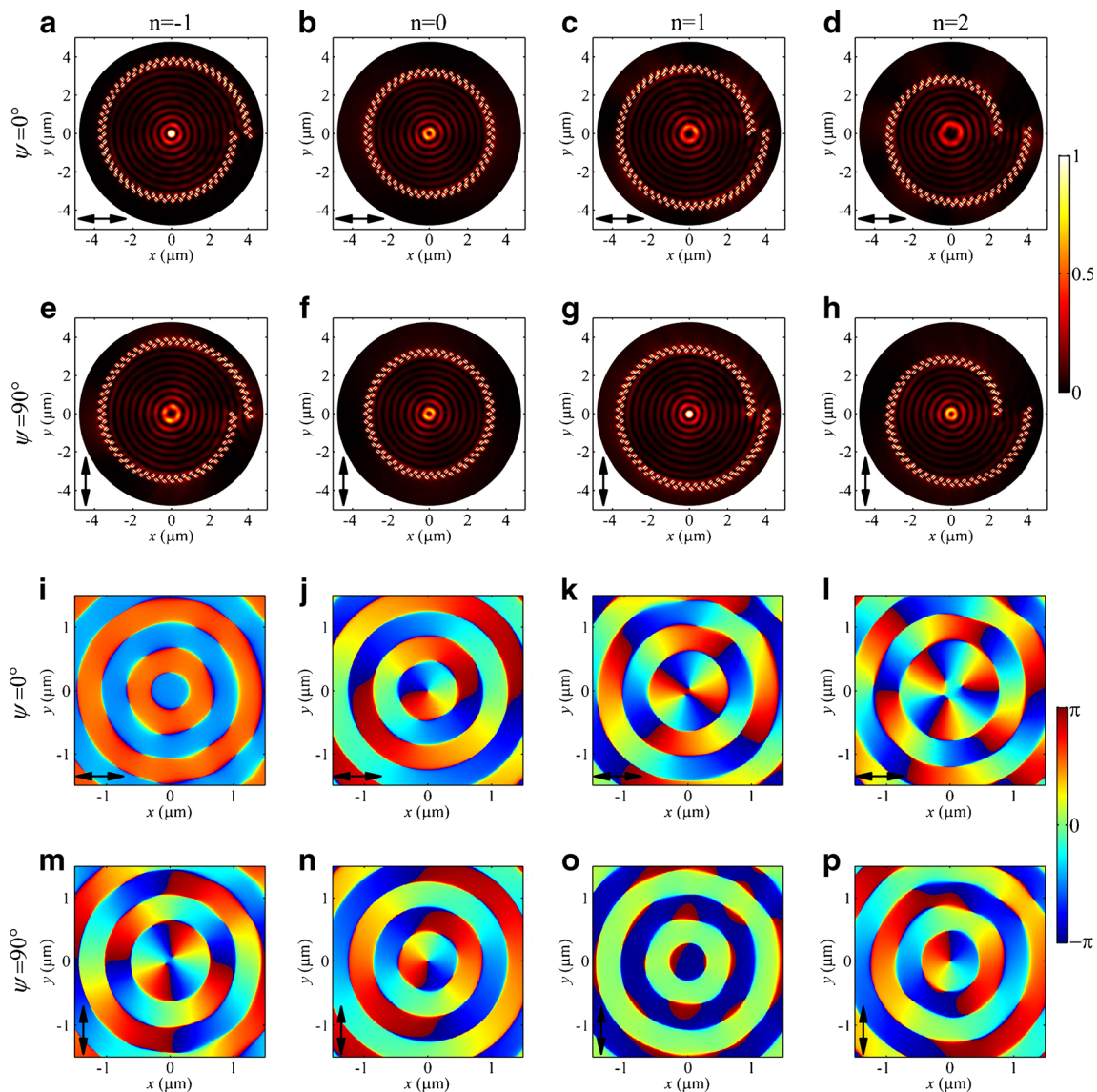


Fig. 2a–h Simulated intensity $|E_z|^2$ distributions at $z=0$ plane for $n = -1$ to 2 with $\psi = 0^\circ$ and 90° linear polarization incidence. **i–p** Simulated E_z filed phase distributions at $z=0$ plane correspond to (a–h). The angle α_0

is 45° . The arrows in this figure and the figures below indicate the polarization directions of the incident light

linearly polarized incident light. Further changing the rotating direction of the Archimedes curves, as shown in Fig. 3b, f, the plasmonic vortex returns to +2 ordered. In addition, the intensity distributions for $\alpha_0 = 0^\circ$ are shown in Fig. 3c, d. When the incident light is 45° and 135° linearly polarized, the TCs of generated plasmonic vortex are 0 and +2, respectively. The E_z phase distributions at $z=0$ plane which correspond to Fig. 3a–d are shown in Fig. 3e–h, respectively.

To make the plasmonic lens have comparable size, the minimum radiuses r_0 for $n = -1$ to 2 in Fig. 2 are set to be $5\lambda_{\text{SPP}}$, $4\lambda_{\text{SPP}}$, $4\lambda_{\text{SPP}}$, and $3\lambda_{\text{SPP}}$, respectively. For higher-ordered plasmonic vortex, the pitch of the plasmonic lens needs to be increased; thus, the size of the

plasmonic lens must be increased. A better solution for generating higher-ordered plasmonic vortex is to cut the continuous Archimedes curves into segments, which can be described as follows:

$$r = r_0 + \frac{n\lambda_{\text{SPP}}}{2\pi} \bmod(m\phi, 2\pi) \quad (8)$$

where m is an integer that denotes the number of the segments and $\bmod(m\phi, 2\pi)$ represents the remainder of the division of $m\phi$ by 2π . The integrating result of Eq. (6) could be as follows [22]:

$$\vec{E}_{\text{SPP}}(R, \theta) = \mp \hat{z} \sqrt{2\pi} E_0 C e^{-k_z z} r_0 e^{i(k_{\text{SPP}} r_0 \pm \alpha_0)} e^{i(m \times n \pm 1)\theta} J_{m \times n \pm 1}(k_{\text{SPP}} R) \quad (9)$$

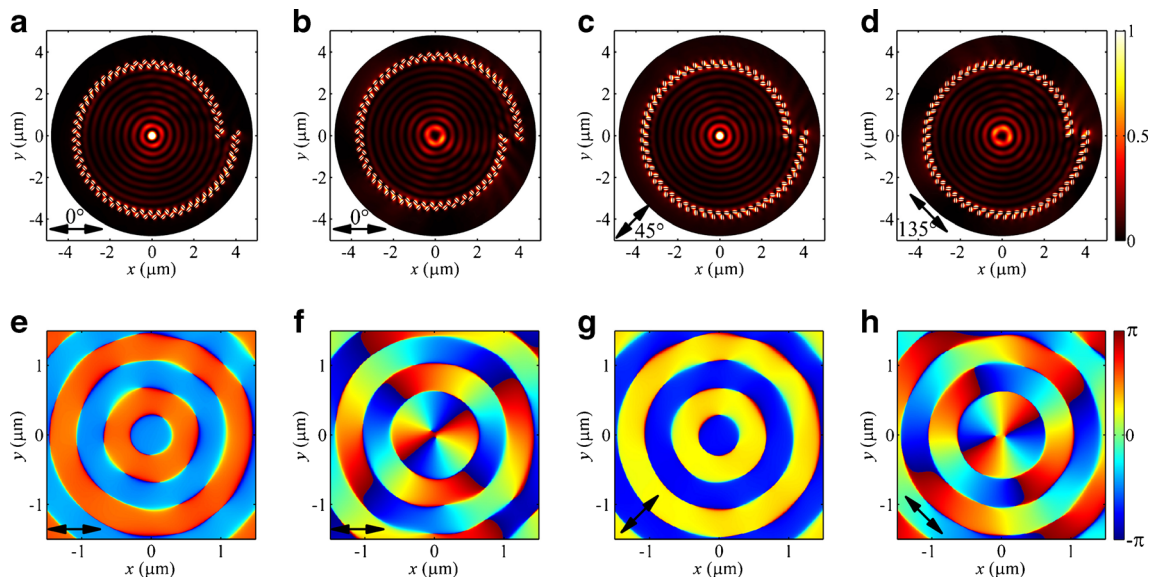


Fig. 3 **a** Intensity distribution at $z=0$ plane with $n=1$ and $\psi=0^\circ$ linearly polarized incident light, where the orientation of all nanoslits is altered by 90° with respect to those in Fig. 2c. **b** Intensity distribution when further changing the rotating direction of the Archimedes curves. **c–d** Intensity

distributions for $\alpha_0=0^\circ$ with 45° (**e**) and 135° (**d**) linearly polarized incident light, respectively. **e–h** E_z phase distributions correspond to (**a–d**), respectively

The TC of generated plasmonic vortex is $m \times n \pm 1$. By combination the geometric parameters m and n , plasmonic vortex with high TC could be generated with small plasmonic lens size. The simulated results for $m=2$ and 3 are typically shown in Fig. 4. The nanoslits in the inner and outer arrays are oriented at angles 45° and 135° with respect to the x axis, respectively ($\alpha_0=45^\circ$). The first row of Fig. 4 shows the intensity $|E_z|^2$ distributions at $z=0$ plane with $(m, n) = (2, 1)$ and $(3, 2)$ for 90° and 0°

linear polarization incidence, respectively. The corresponding phase distributions are shown in Fig. 4e–h. In order to better illustrate the TC of generated plasmonic vortex, the centers are blocked with solid circles in the phase maps [22]. The TC of the generated plasmonic vortex is 1 to 7 with an increment of 2. The minimum radiuses for $(m, n) = (2, 1)$ and $(3, 2)$ are $4\lambda_{SPP}$ and $3\lambda_{SPP}$, respectively. The maximum radiuses for these two plasmonic lens are both only $5\lambda_{SPP}$.

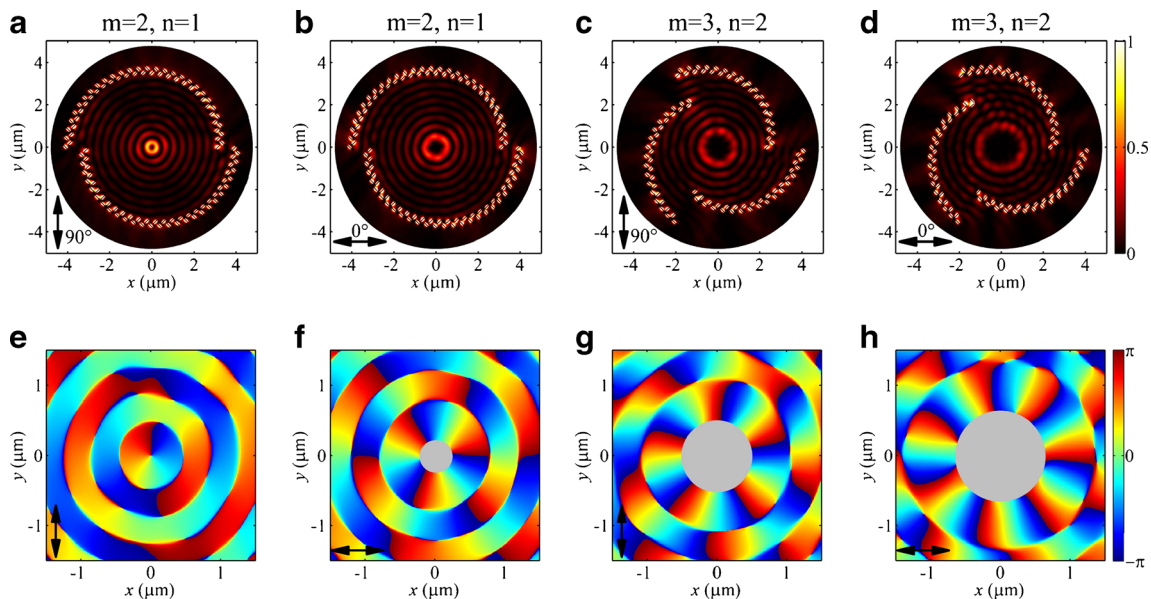
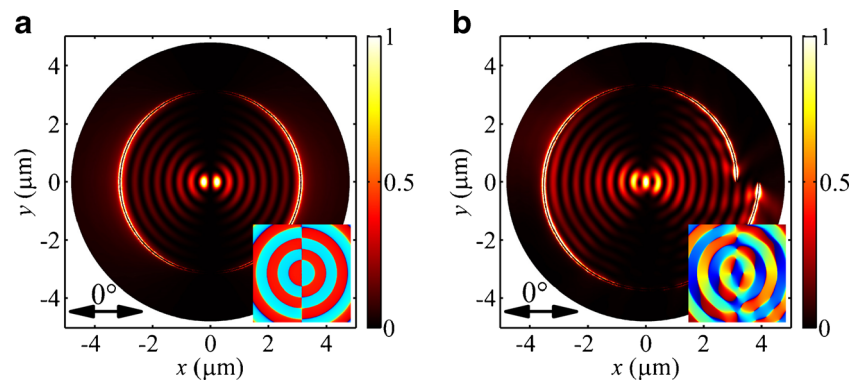


Fig. 4 **a–d** Intensity distributions at $z=0$ plane with $(m, n) = (2, 1)$ and $(3, 2)$ for 90° and 0° linear polarization incidence, respectively. **e–h** E_z phase distributions correspond to (**a–d**)

Fig. 5 **a** Simulated intensity distributions at $z=0$ plane for a circular plasmonic lens. The radius of the ring is $4\lambda_{\text{SPP}}$. **b** Simulated intensity distribution for an Archimedes spiral plasmonic lens. The Archimedes curve is $r = 4\lambda_{\text{SPP}} + \lambda_{\text{SPP}}\phi/2\pi$. Both of the nanoslit widths are 60 nm. *Insets* shows the phase distributions. The incident light is 0° linearly polarized



Till now, we have shown that the proposed plasmonic lens can generate plasmonic vortex with linearly polarized incident light. The TC of the generated plasmonic vortex is determined by the polarization state of incident light, the geometric parameters n and m , which are the pitch of the plasmonic lens in the units of λ_{SPP} and the number of Archimedes curves segments, respectively, and the orientation angles of the nanoslits. Different combinations of the geometry parameters and the polarization direction of the linearly polarized incident light could flexibly generate plasmonic vortex field with arbitrary TC. At last, the unique properties of the proposed plasmonic lens in plasmonic vortex generation can be clearer by comparing with a circular slit plasmonic lens and an Archimedes spiral slit plasmonic lens. The intensity distributions at $z=0$ plane for these two plasmonic lenses with 0° linearly polarized incident light are shown in Fig. 5a, b, respectively. Because of the geometric phase [6], the SPP interfere destructively at the center of the circular slit plasmonic lens, leading to a dark center, while SPP interfere constructively at the center of the Archimedes spiral slit plasmonic lens, leading to a bright spot at the center. For these two plasmonic lenses, due to the SPP excitation polarization sensitivity, the intensity distributions inside the plasmonic lenses are inhomogeneous along the azimuth direction and are proportional to $\cos^2\phi$. Moreover, the E_z field phase distributions at $z=0$ plane for these two plasmonic lenses are shown within the insets of Fig. 5a, b, respectively. The phase distributions are not linearly changing with the azimuthal angle. The inhomogeneous intensity distributions and nonlinear phase variation along the azimuthal direction indicate that these two plasmonic lenses cannot generate plasmonic vortex with linearly polarized incident light.

Conclusion

In conclusion, a plasmonic lens which consists of two arrays of nanoslits bent to Archimedes curves and can

generate plasmonic vortex with linearly polarized light is theoretically and numerically investigated. With the proposed plasmonic lens, additional angular momentum of ± 1 is generated with linearly polarized incident light. The TC of the generated plasmonic vortex by this plasmonic lens is found to be the sum of the geometrical charge and the additional angular momentum. It is shown that the generated plasmonic vortex depends on the pitch of the plasmonic lens, the nanoslit orientation directions, and the polarization direction of incident light. Combination of the geometry parameters and the polarization direction of linearly polarized incident light could flexibly generate plasmonic vortex with arbitrary TC. Moreover, by cutting the continuous Archimedes curves into segments, highly ordered plasmonic vortices are realized with a small plasmonic lens size. At last, two slit plasmonic lenses illuminated with linearly polarized light are simulated to demonstrate the unique superiority of the proposed plasmonic lens in plasmonic vortex generation. The flexible method to generate plasmonic vortex with the proposed plasmonic lens may have potential applications in optical trapping, optical data storage, nanoscale microscopy, and quantum computing.

Acknowledgments This work was supported by the National Key Basic Research Program of China (Grant 2013CB328702) and the National Natural Science Foundation of China (Grants 11374074 and 11176009).

References

1. Maier SA (2007) Plasmonics: fundamentals and applications. Springer,
2. Gramotnev DK, Bozhevolnyi SI (2010) Plasmonics beyond the diffraction limit. *Nat Photonics* 4(2):83–91
3. Pan L, Park Y, Xiong Y, Ulin-Avila E, Wang Y, Zeng L, Xiong S, Rho J, Sun C, Bogy DB (2011) Maskless plasmonic lithography at 22 nm resolution. *Sci Report* 1:175

4. Homola J, Dostálek J (2006) Surface plasmon resonance based sensors, vol 4. Springer,
5. Atwater HA, Polman A (2010) Plasmonics for improved photovoltaic devices. *Nat Mater* 9(3):205–213
6. Berry MV (1987) The adiabatic phase and Pancharatnam's phase for polarized light. *J Mod Opt* 34(11):1401–1407. doi:10.1080/09500348714551321
7. Cho S-W, Park J, Lee S-Y, Kim H, Lee B (2012) Coupling of spin and angular momentum of light in plasmonic vortex. *Opt Express* 20(9):10083–10094. doi:10.1364/oe.20.010083
8. Ku C-T, Lin H-N, Huang C-B (2015) Direct observation of surface plasmon vortex and subwavelength focusing with arbitrarily-tailored intensity patterns. *Appl Phys Lett* 106(5):053112. doi:10.1063/1.4907652
9. Lee SY, Kim SJ, Kwon H, Lee B (2015) Spin-direction control of high-order plasmonic vortex with double-ring distributed nanoslits. *IEEE Photon Technol Lett* 27(7):705–708
10. Kim H, Park J, Cho SW, Lee SY, Kang M, Lee B (2010) Synthesis and dynamic switching of surface plasmon vortices with plasmonic vortex lens. *Nano Lett* 10(2):529–536. doi:10.1021/nl903380j
11. Dal Negro L, Lawrence N, Trevino J (2012) Analytical light scattering and orbital angular momentum spectra of arbitrary Vogel spirals. *Opt Express* 20(16):18209–18223. doi:10.1364/OE.20.018209
12. Lawrence N, Trevino J, Negro LD (2012) Control of optical orbital angular momentum by Vogel spiral arrays of metallic nanoparticles. *Opt Lett* 37(24):5076–5078. doi:10.1364/OL.37.005076
13. Li Z, Zhang M, Liang G, Li X, Chen X, Cheng C (2013) Generation of high-order optical vortices with asymmetrical pinhole plates under plane wave illumination. *Opt Express* 21(13):15755–15764. doi:10.1364/OE.21.015755
14. Genevet P, Yu NF, Aieta F, Lin J, Kats MA, Blanchard R, Scully MO, Gaburro Z, Capasso F (2012) Ultra-thin plasmonic optical vortex plate based on phase discontinuities. *Appl Phys Lett* 100(1):3. doi:10.1063/1.3673334
15. Juan ML, Righini M, Quidant R (2011) Plasmon nano-optical tweezers. *Nat Photonics* 5(6):349–356. doi:10.1038/nphoton.2011.56
16. Liu J, Gao Y, Ran L, Guo K, Lu Z, Liu S (2015) Focusing surface plasmon and constructing central symmetry of focal field with linearly polarized light. *Appl Phys Lett* 106(1):013116. doi:10.1063/1.4905307
17. Liu ZW, Steele JM, Srituravanich W, Pikus Y, Sun C, Zhang X (2005) Focusing surface plasmons with a plasmonic lens. *Nano Lett* 5(9):1726–1729. doi:10.1021/nl051013j
18. Shen Z, Hu ZJ, Yuan GH, Min CJ, Fang H, Yuan XC (2012) Visualizing orbital angular momentum of plasmonic vortices. *Opt Lett* 37(22):4627–4629. doi:10.1364/OL.37.004627
19. Shitrit N, Nechayev S, Kleiner V, Hasman E (2012) Spin-dependent plasmonics based on interfering topological defects. *Nano Lett* 12(3):1620–1623. doi:10.1021/nl204556r
20. Yang S, Chen W, Nelson RL, Zhan Q (2009) Miniature circular polarization analyzer with spiral plasmonic lens. *Opt Lett* 34(20):3047–3049
21. Chen WB, Abeysinghe DC, Nelson RL, Zhan QW (2010) Experimental confirmation of miniature spiral plasmonic lens as a circular polarization analyzer. *Nano Lett* 10(6):2075–2079. doi:10.1021/nl100340w
22. Rui GH, Zhan QW, Cui YP (2015) Tailoring optical complex field with spiral blade plasmonic vortex lens. *Sci Report* 5:13732. doi:10.1038/srep13732
23. Chen CF, Ku CT, Tai YH, Wei PK, Lin HN, Huang CB (2015) Creating optical near-field orbital angular momentum in a gold metasurface. *Nano Lett* 15(4):2746–2750. doi:10.1021/acs.nanolett.5b00601
24. Spektor G, David A, Gjonaj B, Bartal G, Orenstein M (2015) Metafocusing by a metaspiral plasmonic lens. *Nano Lett* 15(9):5739–5743. doi:10.1021/acs.nanolett.5b01571
25. Lin J, Mueller JB, Wang Q, Yuan G, Antoniou N, Yuan X-C, Capasso F (2013) Polarization-controlled tunable directional coupling of surface plasmon polaritons. *Science* 340(6130):331–334
26. Lee S-Y, Kim K, Kim S-J, Park H, Kim K-Y, Lee B (2015) Plasmonic meta-slit: shaping and controlling near-field focus. *Optica* 2(1):6–13. doi:10.1364/OPTICA.2.000006
27. Johnson PB, Christy R-W (1972) Optical constants of the noble metals. *Phys Rev B* 6(12):4370